

A New Nonlinear Double-Capacitor Model for Rechargeable Batteries

Ning Tian

University of Kansas

Lawrence, KS 66045, USA

Email: ning.tian@ku.edu

Huazhen Fang

University of Kansas

Lawrence, KS 66045, USA

Email: fang@ku.edu

Jian Chen

Zhejiang University

Hangzhou, China, 310027

Email: jchen@zju.edu.cn

Abstract—This paper proposes a new equivalent circuit model for rechargeable batteries by modifying a double-capacitor model proposed in [1]. It is known that the original model, when compared to other equivalent circuit models, can better address the rate capacity effect and energy recovery effect inherent to batteries. However, it is a purely linear model and includes no representation of a battery’s nonlinear phenomena. Hence, this work transforms the original model by introducing a nonlinear-mapping-based voltage source, with the modification justified by an analysis and comparison with the single-particle model. The new nonlinear double-capacitor model is evaluated extensively, with a parameter identification method proposed and validation performed on a number of experimental datasets. The evaluation shows that the proposed model offers excellent predictive capability. With high fidelity and low mathematical complexity, the proposed new model is advantageous for real-time battery management applications.

I. INTRODUCTION

Rechargeable batteries have seen an ever-increasing use in today’s industry and society as power sources for systems of different scales. This trend has motivated growing research on advanced battery management algorithms. Since such algorithms often hinge on mathematical models that can well capture a battery’s dynamics, battery modeling has attracted incessant interest during the past years. Based on the fundamental modeling principles, the existing battery models generally fall into two categories. The first category builds on electrochemical principles to characterize the electrochemical reactions and physical phenomena inside a battery during charging/discharging [2]. The electrochemical models are considered as the most accurate to predict a battery’s behavior, finding wide use in battery design and analysis. However, involving many partial differential equations, they have complex structures and induce high computational costs. Although a simplified electrochemical model known as single-particle model (SPM) has been developed [3], it is still too sophisticated and computationally expensive when it comes to real-time battery management.

Rather than using electrochemical principles, another popular means of battery modeling is to replicate a battery’s input–output characteristics using circuits made of resistors, capacitors and voltage sources. This leads to a second category that is referred to as equivalent circuit models (ECMs). There is a long history of using ECMs to delineate the internal resistance of batteries. The first one to our knowledge is the

Randles model proposed in the 1940s [4]. It introduces the electrical ohmic and reactive resistance to account for the voltage dynamics in a lead-acid battery. This model has become a de facto standard for interpreting battery data obtained from electrochemical impedance spectroscopy [5]. Adding a voltage source representing the open-circuit voltage (OCV) to the Randles model, one can obtain the Thevenin’s model [6]–[8]. Removing its resistance-capacitance (RC) circuit, the Thevenin’s model reduces to the simple Rint model that includes an ideal voltage source with a series resistor [6]. Adding one or more RC circuits to the series, it becomes the PNGV model capable of capturing multi-time-scale voltage transients during charging/discharging [6]. The literature has also reported a few other modifications to the Thevenin’s model toward grasping a battery’s dynamics at a more sophisticated level [9]–[16]. Another ECM that is emerging as a useful tool is a double-capacitor model [1], [17], which is also referred to as RC model. It uses two capacitors for storing charge. The capacitors differ significantly in capacitance and are configured in parallel, imitating an electrode’s bulk inner part and surface region, respectively. Compared to the Thevenin’s model, this unique circuit structure allows the rate capacity effect and charge recovery effect to be captured, making this model an attractive choice for charging control [18], [19]. Overall, ECMs offer significant mathematical simplicity because of the concise circuit structures and fewer parameters while providing satisfactory predictive capabilities. This has made them conducive to real-time estimation and control and thus advantageous for embedded battery management.

In spite of a large body of work, the development of ECMs has not been fully explored. One of the most pressing is to improve the quality of the double-capacitor model mentioned above. Despite the apparent advantages, this model suffers a major drawback—it has a linear structure and hence cannot describe a battery’s nonlinear behavior. In particular, it is unable to capture the nonlinear SoC-OCV relationship, which is critical for predicting a battery’s voltage behavior. To deal with this issue, this paper presents a new ECM by improving on the double-capacitor model, through a systematic effort of model development, identification and validation. The specific contributions of this paper are outlined as follows. First, the double-capacitor model is modified by introducing a voltage source as a nonlinear mapping of the voltage across the surface

capacitor. Such a modification has never been reported but can be well justified by drawing an analogy to the SPM. It transforms the original model to allow the nonlinear voltage dynamics to be simulated by the circuit. As a result, the new model, which is named nonlinear double-capacitor (NDC) model, is physically more reasonable and can offer remarkably improved predictive accuracy. Second, an extensive validation is performed to evaluate the NDC model. To this end, a method is presented to identify the model parameters from measurement data in one shot. The obtained model is then applied to different experimental datasets, where an excellent prediction performance is observed. With the effectiveness and mathematical conciseness, the proposed model may find significant prospective use in advanced battery management.

The remainder of the paper is organized as follows. Section II presents the development of the new NDC model based on modifying the original double-capacitor model. Section III analyzes and reveals the model parameter's local identifiability and presents an identification method for the parameter estimation. Section IV offers numerical simulation to verify the model parameter identifiability and gives the fundamental upper limit for parameter estimation accuracy. Section V validates the prediction performance of the proposed NDC model using different datasets. Finally, concluding remarks are gathered in Section VI.

II. NDC MODEL DEVELOPMENT

This section develops the new NDC model based on the traditional double-capacitor model and presents the mathematical equations governing its dynamics.

As shown in Figure 1(a), the double-capacitor model includes two capacitors in parallel, C_b and C_s , each serially connected with a resistor, R_b and R_s , respectively. The double capacitors provide storage for electric charge like an electrode and when parallelly connected, simulate the distribution and migration of charge within the electrode. Specifically, the R_s - C_s circuit can be considered as corresponding to the electrode surface region exposed to the electrode-electrolyte interface; the R_b - C_b circuit represents an analogy of the bulk inner part of the electrode. This hence implies $C_b \gg C_s$ and $R_b \gg R_s$. It can be seen that C_b is where the majority of the charge is stored and that R_b - C_b would demonstrate the low-frequency part of the charging/discharging response. By contrast, C_s has a capacity much less than C_b , and its voltage shows a much faster change during charging/discharging. This indicates that the R_s - C_s circuit is responsible for the high-frequency response. In addition, R_0 is included into the circuit to account for the electrolyte resistance. It is pointed out in [18] that this model can grasp the rate capacity effect, i.e., the total charge absorbed (or released) by a battery goes down with the increase in charging (or discharging) current. To see this, it should be noticed that V_s , the voltage across C_s , changes faster than V_b , the voltage across C_b , and that the terminal voltage V is mainly affected by V_s . Thus, when the current I is large, the fast rise (or decline) of V_s will make V hit the cut-off threshold earlier even though C_b has yet to be

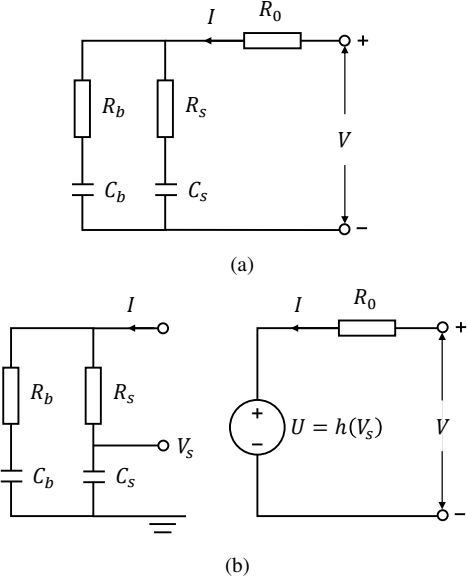


Figure 1: (a) The original double-capacitor model; (b) the proposed nonlinear double-capacitor model.

fully charged (or discharged). Another phenomenon that can be captured is the capacity and voltage recovery effect. That is, the usable capacity and terminal voltage would increase upon the termination of discharging due to the migration of charge from C_b to C_s .

However, with the nature of a linear dynamic system, this model is unable to describe the nonlinear dependence of a battery's OCV on SoC, which is a crucial feature of batteries. Its application is thus restricted to only a limited SoC range allowing for a linear approximation of the SoC-OCV curve, which would impose much conservatism on the use of a battery. To overcome this issue, the NDC model is proposed to expand the original model to include a nonlinear mapping of V_s , as shown in Figure 1(b). The mapping, expressed as $U = h(V_s)$, is equivalent to a voltage source, which directly affects the terminal voltage V .

Here, let us justify the above modification from a perspective of the SPM, a simplified electrochemical model that has recently attracted wide interest. An analysis in [18] reveals an approximate mathematical equivalence between the double-capacitor model and the SPM in terms of the transport of the lithium ions within an electrode. The SPM represents an electrode as a spherical particle, within which lithium ions are stored. A charging/discharging process would drive a diffusion-based migration of the lithium ions within the electrode. If subdividing a spherical particle into two finite volumes, the bulk inner domain and the near-surface domain, one can simplify the diffusion of lithium ions between them to a form approximately equivalent to that of the charge transport for the double-capacitor model, as proven in [18]. For SPM, the terminal voltage depends on three factors: the difference in the open-circuit potential of the positive and negative electrodes, the difference in the reaction overpotential, and the voltage across the film resistance [2]. The reaction

overpotential difference is almost negligible when the input current is not too large. In addition, the open-circuit potential depends on the lithium-ion concentration in the surface region of the sphere, which is akin to the charge amount on C_s and consequently relates to the voltage of C_s , i.e., V_s . Therefore, it is appropriate as well as necessary to introduce a nonlinear function of V_s as an analogy to the between-electrode open-circuit potential difference. This comparison with the SPM suggests that the NDC model is physically reasonable. With the proposed change, this new model can correctly show the influence of the charge state on the terminal voltage, while inheriting all the capabilities of the original model.

For the NDC model, $h(V_s)$ can be parameterized as a polynomial. A fifth-order polynomial is considered here, i.e.,

$$h(V_s) = \alpha_0 + \alpha_1 V_s + \alpha_2 V_s^2 + \alpha_3 V_s^3 + \alpha_4 V_s^4 + \alpha_5 V_s^5,$$

where α_i for $i = 0, 1, \dots, 5$ are coefficients. Then, the model dynamics can be expressed as follows:

$$\begin{cases} \begin{bmatrix} \dot{V}_b(t) \\ \dot{V}_s(t) \end{bmatrix} = A \begin{bmatrix} V_b(t) \\ V_s(t) \end{bmatrix} + BI(t), \\ V(t) = h(V_s(t)) + R_0 I(t), \end{cases} \quad (1a)$$

$$(1b)$$

where

$$A = \begin{bmatrix} -\frac{1}{C_b(R_b+R_s)} & \frac{1}{C_b(R_b+R_s)} \\ \frac{1}{C_s(R_b+R_s)} & -\frac{1}{C_s(R_b+R_s)} \end{bmatrix}, \quad B = \begin{bmatrix} \frac{R_s}{C_b(R_b+R_s)} \\ \frac{R_b}{C_s(R_b+R_s)} \end{bmatrix}.$$

In above, $I > 0$ for charging, and $I < 0$ for discharging. Note that V_b and V_s should be set to belong to an interval $[\underline{V}_s, \bar{V}_s]$. Here, let $\underline{V}_s = 0$ V and $\bar{V}_s = 1$ V for simplicity. Then, $V_b = V_s = 1$ V for full charge (100% of SoC), and $V_b = V_s = 0$ V for full depletion (0% of SoC). Further, the SoC can be calculated by

$$\text{SoC} = \frac{C_b V_b + C_s V_s}{C_b + C_s} \times 100\%,$$

where $C_b + C_s$ is the total capacity, and $C_b V_b + C_s V_s$ the available capacity.

The rest of this paper will center on assessing the predictive performance of the NDC model. To achieve this, a parameter identification method will be developed to determine the model parameters using discharging data. This is followed by applying the identified model to diverse experimental datasets.

III. PARAMETER IDENTIFICATION

This section is focused on one-shot parameter identification for the NDC model. It begins with analyzing the voltage response under constant discharge current and the local parameter identifiability. An identification method is then presented.

A. Terminal Voltage Response Analysis

Consider a battery fully charged and left idling for a long period of time, and then fully discharge it using a constant current I . According to (1a), V_s is

$$\begin{aligned} V_s(t) = V_s(0) + \frac{It}{C_b + C_s} + \frac{C_b(R_b C_b - R_s C_s)I}{(C_b + C_s)^2} \\ \cdot \left[1 - \exp \left(-\frac{C_b + C_s}{C_b C_s (R_b + R_s)} t \right) \right], \end{aligned} \quad (2)$$

where $V_s(0) = 1$ is the initial value of V_s at full charge state. The response of the terminal voltage V then follows (1b). However, as pointed out in [20], it is not possible to identify C_b , R_b , C_s and R_s altogether. This issue can also be seen from (2), where V_s depends on three combined parameters, i.e., $1/(C_b + C_s)$, $C_b(R_b C_b - R_s C_s)/(C_b + C_s)^2$, and $(C_b + C_s)/[C_b C_s (R_b + R_s)]$. Even if they are determined, no one can extract all the four individual RC parameters from them. A straightforward way to avoid this issue is to assume $R_s = 0$, as suggested and used in [20]. This assumption is tenable with $R_s \ll R_b$ for the NDC model. As a result, (2) becomes

$$\begin{aligned} V_s(t) = 1 + \frac{It}{C_b + C_s} + \frac{R_b C_b^2 I}{(C_b + C_s)^2} \\ \cdot \left[1 - \exp \left(-\frac{C_b + C_s}{C_b C_s R_b} t \right) \right]. \end{aligned} \quad (3)$$

Further, it is reasonable to assume that $V_s(t_{\text{end}}) = \underline{V}_s = 0$ V when the terminal voltage V hits the lower cut-off threshold, where t_{end} is the end time of discharging. For most batteries, if the discharging current is not extremely large and t_{end} is long enough, then

$$\exp \left(-\frac{C_b + C_s}{C_b C_s R_b} t_{\text{end}} \right) \approx 0.$$

Hence, one has

$$\frac{R_b C_b^2 I}{(C_b + C_s)^2} \approx -1 - \frac{It_{\text{end}}}{C_b + C_s}. \quad (4)$$

As a result, (3) can further reduce to

$$V_s(t) = 1 + \beta_1 I t - (1 + \beta_1 I t_{\text{end}}) (1 - e^{-\beta_2 t}),$$

where

$$\beta_1 = \frac{1}{C_b + C_s}, \quad \beta_2 = \frac{C_b + C_s}{C_b C_s R_b}.$$

When obtained, β_1 and β_2 , together with (4) can be used to calculate C_b , C_s and R_b as follows:

$$C_b = \frac{1}{\beta_1(\beta_3 + 1)}, \quad C_s = \frac{\beta_3}{\beta_1(\beta_3 + 1)}, \quad R_b = \frac{\beta_1(\beta_3 + 1)^2}{\beta_2 \beta_3},$$

where

$$\beta_3 = -\frac{\beta_1 I}{\beta_2 + \beta_1 \beta_2 I t_{\text{end}}}.$$

An additional piece of information is worth noting here. That is, the initial terminal voltage $V(0)$ satisfies $V(0) = h(V_s(0) = 1) = \sum_{i=0}^5 \alpha_i$ in the considered setting. Then, by letting α_0 by $\alpha_0 = V(0) - \sum_{i=1}^5 \alpha_i$, one can take off α_0 from identification, reducing one parameter to be estimated.

The above analysis leads us to the following characterization of the terminal voltage V under constant-current discharging:

$$V(\boldsymbol{\theta}; t) = V(0) - \sum_{i=1}^5 \theta_i + \sum_{i=1}^5 \theta_i V_s^i(\boldsymbol{\theta}; t) + I \theta_8, \quad (5)$$

where

$$\boldsymbol{\theta} = [\alpha_1 \ \alpha_2 \ \alpha_3 \ \alpha_4 \ \alpha_5 \ \beta_1 \ \beta_2 \ R_0]^\top,$$

$$V_s(\boldsymbol{\theta}; t) = 1 + \theta_6 I t - (1 + \theta_6 I t_{\text{end}}) (1 - e^{-\theta_7 t}).$$

Note that θ_i for $i = 1, 2, \dots, 8$ and its corresponding parameter will be used interchangeably in sequel.

B. Identifiability Analysis and Identification

Identifiability analysis is to determine whether the parameters of a model can be uniquely extracted from measurement data. Loosely speaking, parameters are called globally identifiable if there do not exist two different parameter sets anywhere in the parameter space to satisfy a same data sequence, implying the parameter sets are “differentiable”. They are locally identifiable if the differentiability only holds in the neighborhood of a nominal point. A rigorous definition of local identifiability can be found in [21]. A common method for investigating identifiability is performing sensitivity analysis, which, as indicated in [21], [22], is to check if the sensitivity matrix $\mathbf{S}(\boldsymbol{\theta})$ has full rank. If so, $\boldsymbol{\theta}$ is considered to be locally identifiable. From (5), $\mathbf{S}(\boldsymbol{\theta})$ can be derived as follows

$$\mathbf{S}(\boldsymbol{\theta}) = \begin{bmatrix} \vdots & \vdots & \vdots & \vdots \\ \frac{\partial V(\boldsymbol{\theta}; t_k)}{\partial \theta_1} & \frac{\partial V(\boldsymbol{\theta}; t_k)}{\partial \theta_2} & \dots & \frac{\partial V(\boldsymbol{\theta}; t_k)}{\partial \theta_8} \\ \vdots & \vdots & \vdots & \vdots \end{bmatrix}_{N \times 8},$$

where

$$\begin{aligned} \frac{\partial V(\boldsymbol{\theta}; t_k)}{\partial \theta_i} &= V_s^i(\boldsymbol{\theta}; t_k) - 1, \text{ for } i = 1, 2, \dots, 5, \\ \frac{\partial V(\boldsymbol{\theta}; t_k)}{\partial \theta_6} &= \left(\sum_{j=1}^5 j \theta_j V_s^{j-1}(\boldsymbol{\theta}; t_k) \right) \\ &\quad \cdot (I t_k - I t_{\text{end}} + I t_{\text{end}} e^{-\theta_7 t_k}), \\ \frac{\partial V(\boldsymbol{\theta}; t_k)}{\partial \theta_7} &= - \left(\sum_{j=1}^5 j \theta_j V_s^{j-1}(\boldsymbol{\theta}; t_k) \right) \\ &\quad \cdot (1 + \theta_6 I t_{\text{end}}) t_k e^{-\theta_7 t_k}, \\ \frac{\partial V(\boldsymbol{\theta}; t_k)}{\partial \theta_8} &= I. \end{aligned}$$

In above, t_k denotes the sampling time instants, and the total number is N . By observation, one can see that the columns of $\mathbf{S}(\boldsymbol{\theta})$ are linearly independent if given a nominal point $\boldsymbol{\theta} = \boldsymbol{\theta}_0$, implying that the matrix is of full rank. This observation is further verified through numerical simulation in Section IV. Hence, $\boldsymbol{\theta}$ is concluded to be locally identifiable.

Consider identification of $\boldsymbol{\theta}$ using the prediction-error method, which means to find out the parameters to minimize the model-based prediction error. Hence, the following optimization problem can be formulated:

$$\hat{\boldsymbol{\theta}} = \min_{\boldsymbol{\theta}} J(\boldsymbol{\theta}) = \frac{1}{2} [\mathbf{y} - \mathbf{V}(\boldsymbol{\theta})]^\top \mathbf{Q}^{-1} [\mathbf{y} - \mathbf{V}(\boldsymbol{\theta})],$$

where \mathbf{y} is the noise-contaminated measurement vector, \mathbf{Q} a symmetric positive definite matrix interpretable as the covariance of noise additive to $\mathbf{V}(\boldsymbol{\theta})$, and

$$\begin{aligned} \mathbf{y} &= [y(t_1) \ y(t_2) \ \dots \ y(t_N)]^\top, \\ \mathbf{V}(\boldsymbol{\theta}) &= [\mathbf{V}(\boldsymbol{\theta}; t_1) \ \mathbf{V}(\boldsymbol{\theta}; t_2) \ \dots \ \mathbf{V}(\boldsymbol{\theta}; t_N)]^\top. \end{aligned}$$

The above minimization problem can be solved using numerical optimization methods, e.g., the trust-region method.

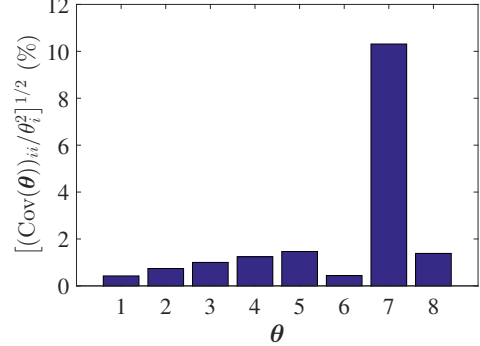


Figure 2: Evaluation of the parameter estimation covariance.

Meanwhile, it is noted as a nonlinear and nonconvex problem. This may put the optimal parameter search at a risk of converging to physically incorrect parameters especially when the initial parameter guess is far from the truth. One way to address it is to constrain the parameter search by setting up the rough upper and lower bounds of certain parameters when they can be decided using some prior knowledge [23].

Consider the nominal parameter vector as $\boldsymbol{\theta}_0$ and suppose that $\hat{\boldsymbol{\theta}}$ minimizes $J(\boldsymbol{\theta})$ successfully. Its covariance in the Gaussian case is given by

$$\text{Cov}(\hat{\boldsymbol{\theta}}) = \mathbb{E} \left(\left[\frac{\partial^2 J(\boldsymbol{\theta})}{\partial \boldsymbol{\theta}^2} \Big|_{\boldsymbol{\theta}_0} \right]^{-1} \right) = [\mathbf{S}^\top(\boldsymbol{\theta}_0) \mathbf{Q}^{-1} \mathbf{S}(\boldsymbol{\theta}_0)]^{-1},$$

from which the variance of the estimate $\hat{\theta}_i$, for $i = 1, 2, \dots, 8$, is the i -th diagonal element of $\text{Cov}(\hat{\boldsymbol{\theta}})$, i.e., $[\text{Cov}(\hat{\boldsymbol{\theta}})]_{ii}$. When evaluating the covariance relative to the parameters’ magnitude, one can consider the scale-normalized covariance:

$$\text{Cov}(\boldsymbol{\Gamma}_{\boldsymbol{\theta}_0}^{-1} \hat{\boldsymbol{\theta}}) = \boldsymbol{\Gamma}_{\boldsymbol{\theta}_0}^{-1} \text{Cov}(\hat{\boldsymbol{\theta}}) \boldsymbol{\Gamma}_{\boldsymbol{\theta}_0}^{-1}, \quad (6)$$

with $\boldsymbol{\Gamma}_{\boldsymbol{\theta}_0} = \text{diag}(\boldsymbol{\theta}_0)$.

IV. NUMERICAL SIMULATION

This section presents numerical simulation to assess the effectiveness of the identifiability analysis and identification method in Section III.

Assume a battery with $C_b = 10,068$ F, $C_s = 1,124$ F, $R_b = 0.0366$ Ω , $R_s = 0$ Ω , $R_0 = 0.113$ Ω , and $h(V_s)$ follows

$$\begin{aligned} h(V_s) &= 2.88 + 6.144V_s - 23.39V_s^2 + 48.5V_s^3 \\ &\quad - 46.86V_s^4 + 16.87V_s^5. \end{aligned} \quad (7)$$

The corresponding parameter vector is

$$\boldsymbol{\theta} = [6.144 \ -23.39 \ 48.5 \ -46.86 \ 16.87 \ 8.935 \times 10^{-5} \ 0.027 \ 0.113]^\top. \quad (8)$$

Suppose that the battery at first is fully charged with the terminal voltage $V = 4.144$ V. Then it is discharged using a constant current of 3 A until $V_s = 0$ V. The measurement \mathbf{V} is subject to zero-mean Gaussian additive noise with covariance of $\mathbf{Q} = 10^{-4} \mathbf{I}$.

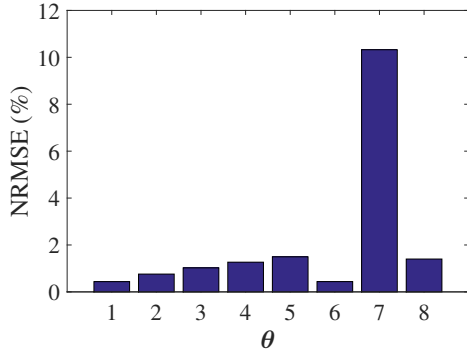


Figure 3: Normalized root-mean-square error for θ .

Computational verification shows that the sensitivity matrix $S(\theta)$ for this battery around the true parameters has full rank, confirming that θ is locally identifiable. Then, one can use (6) to calculate the expected parameter estimation error covariance, which is depicted in Figure 2. The covariance can be interpreted as ratio-based parameter estimation error relative to the parameter magnitude, thus indicating the estimation accuracy. From Figure 2, it is seen that estimation error is below 2% for all parameter except θ_7 .

Monte Carlo simulation is performed to further evaluate the accuracy of parameter identification. In a simulation run, synthetic I - V data is generated using the model with measurement noise incorporated. The initial guess θ_{guess} is set to be

$$\theta_{\text{guess}} = [1 \ 1 \ 1 \ 1 \ 1 \ 8 \times 10^{-5} \ 0.03 \ 0.1]^\top. \quad (9)$$

The identification procedure proposed in Section III-B is then applied to the data to identify the parameters. The simulation is repeatedly run for $M = 1000$ times. The parameter estimate of each run is recorded and used to calculate the normalized root-mean-square error (NRMSE):

$$\text{NRMSE}_i = \sqrt{\frac{\frac{1}{M} \sum_{k=1}^M (\hat{\theta}_i[k] - \theta_i)^2}{\theta_i^2}},$$

for $i = 1, 2, \dots, 8$, where k denotes the number of the Monte Carlo run. Figure 3 shows the NRMSE of each parameter in θ , which is consistent with the results presented by Figure 2. All these results indicate the effectiveness of the identifiability analysis and identification method in Section III.

V. EXPERIMENTAL VALIDATION

Based on the foregoing sections, this section presents experimental validation of the proposed NDC model.

Our experiments were conducted on a PEC® SBT4050 battery tester. In the experiments, the sampling time interval was 1 s. Using this facility, charging/discharging tests were performed to generate data on a Panasonic NCR18650B Li-ion battery cell, which has a rated capacity of 3.25 Ah. The tests are of two types. The first type was meant to produce a training dataset used to identify the parameters of an NDC model. The training dataset was obtained by discharging the fully charged cell to 2.5 V using a constant current of 3 A.

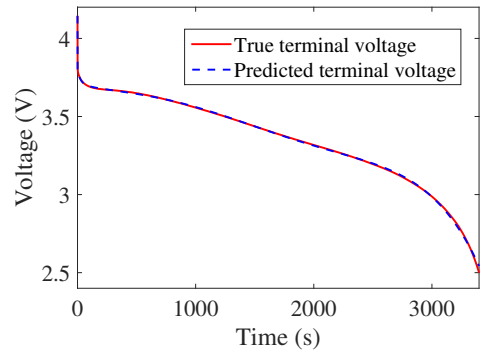


Figure 4: Comparison between the true and predicted voltage under 3 A constant discharging current.

The second type was to yield multiple validation datasets, to which the identified model is applied to assess the predictive capability. The validation datasets were created by discharging the cell using constant currents of 2 A, 2.5 A, 3.5 A, 4 A and 4.5 A and a varying current profile.

To begin with, the training dataset is processed by the identification method in Section III-B to identify and prepare the NDC model for the considered cell. The initial guess of the parameters is set to be the same with that in (9), and the resulting model parameter estimates are the ones shown earlier in (8). That is, $C_b = 10,068$ F, $C_s = 1,124$ F, $R_b = 0.0366$ Ω , $R_s = 0$ Ω , $R_0 = 0.113$ Ω , and $h(V_s)$ follows (7). It is seen that the parameters are practically reasonable and align with our general knowledge of this cell. Besides, Figure 4 compares the model-predicted voltage against the measured, which shows an excellent match between them.

Next, the identified model is applied to validation datasets. The first datasets describe the cell's terminal voltage under constant-current discharging with the currents of 2 A, 2.5 A, 3.5 A, 4 A and 4.5 A. Figure 5 offers the comparison between the measured and model-predicted voltage. One can observe an overall excellent predictive performance. This is obvious especially when the current load nears the current of 3 A used to produce the training dataset. The second batch of datasets demonstrates the voltage behavior under a current load profile generated according to Urban Dynamometer Driving Schedule (UDDS) [24], which is scaled to be between 2.5 A and 3.5 A, see Figure 6(a). The fitting results are given in Figure 6(b), which shows that the model predicted voltage is quite close to the actual measurement.

VI. CONCLUSION

The emergence of real-time battery management has stimulated a demand for battery models striking a balance between fidelity and complexity, making ECMs a primary choice in this field. Compared to many other ECMs, the double-capacitor model promises a few unique advantages for capturing a battery's dynamics. However, its intrinsic linear dynamics hinders a characterization of the nonlinear phenomena. This paper was hence motivated to modify the original double-capacitor model by adding a nonlinear-mapping-based voltage

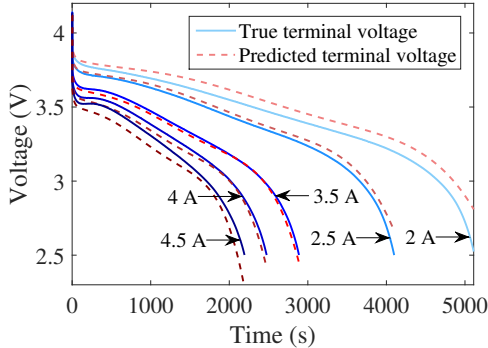


Figure 5: Comparison between the true and predicted voltage under different constant discharging currents.

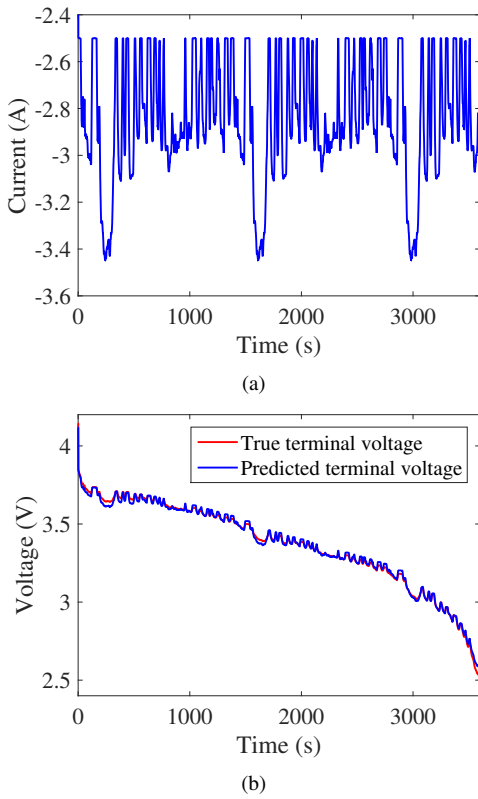


Figure 6: (a) Variable current profile; (b) comparison between the true and predicted voltage.

source. This development was justified through an analogous comparison with the SPM. The proposed new model was then subjected to rigorous evaluation, which includes parameter identification development and experimental validation. The results demonstrated the competence of the proposed model for predicting a battery's behavior.

REFERENCES

- [1] V. H. Johnson and A. A. Pesaran, "Temperature-dependent battery models for high-power lithium-ion batteries," National Renewable Energy Laboratory, Tech. Rep. NREL/CP-540-28716, 2000.
- [2] N. Chaturvedi, R. Klein, J. Christensen, J. Ahmed, and A. Kojic, "Algorithms for advanced battery-management systems," *IEEE Control Systems*, vol. 30, no. 3, pp. 49–68, 2010.
- [3] M. Guo, G. Sikha, and R. E. White, "Single-particle model for a lithium-ion cell: Thermal behavior," *Journal of The Electrochemical Society*, vol. 158, no. 2, pp. A122–A132, 2011.
- [4] J. E. B. Randles, "Kinetics of rapid electrode reactions," *Discussions of the Faraday Society*, vol. 1, pp. 11–19, 1947.
- [5] A. I. Zia and S. C. Mukhopadhyay, *Impedance Spectroscopy and Experimental Setup*. Springer International Publishing, 2016, pp. 21–37.
- [6] S. M. G. and M. Nikdel, "Various battery models for various simulation studies and applications," *Renewable and Sustainable Energy Reviews*, vol. 32, pp. 477–485, 2014.
- [7] H. He, R. Xiong, and J. Fan, "Evaluation of lithium-ion battery equivalent circuit models for state of charge estimation by an experimental approach," *Energies*, vol. 4, pp. 582–598, 2011.
- [8] G. L. Plett, *Battery Management Systems, Volume 1: Battery Modeling*. Artech House, 2015.
- [9] C. Weng, J. Sun, and H. Peng, "A unified open-circuit-voltage model of lithium-ion batteries for state-of-charge estimation and state-of-health monitoring," *Journal of Power Sources*, vol. 258, pp. 228–237, 2014.
- [10] X. Lin, H. E. Perez, S. Mohan, J. B. Siegel, A. G. Stefanopoulou, Y. Ding, and M. P. Castanier, "A lumped-parameter electro-thermal model for cylindrical batteries," *Journal of Power Sources*, vol. 257, pp. 1–11, 2014.
- [11] H. E. Perez, X. Hu, S. Dey, and S. J. Moura, "Optimal charging of Li-ion batteries with coupled electro-thermal-aging dynamics," *IEEE Transactions on Vehicular Technology*, vol. 66, no. 9, pp. 7761–7770, 2017.
- [12] Y. Wang, H. Fang, L. Zhou, and T. Wada, "Revisiting the state-of-charge estimation for lithium-ion batteries: A methodical investigation of the extended Kalman filter approach," *IEEE Control Systems*, vol. 37, no. 4, pp. 73–96, 2017.
- [13] G. L. Plett, "Extended Kalman filtering for battery management systems of LiPB-based HEV battery packs: Part 2. Modeling and identification," *Journal of Power Sources*, vol. 134, no. 2, pp. 262–276, 2004.
- [14] X. Hu, S. Li, and H. Peng, "A comparative study of equivalent circuit models for Li-ion batteries," *Journal of Power Sources*, vol. 198, pp. 359–367, 2012.
- [15] M. Chen and G. A. Rincon-Mora, "Accurate electrical battery model capable of predicting runtime and I-V performance," *IEEE Transactions on Energy Conversion*, vol. 21, no. 2, pp. 504–511, 2006.
- [16] T. Kim and W. Qiao, "A hybrid battery model capable of capturing dynamic circuit characteristics and nonlinear capacity effects," *IEEE Transactions on Energy Conversion*, vol. 26, no. 4, pp. 1172–1180, 2011.
- [17] V. Johnson, "Battery performance models in ADVISOR," *Journal of Power Sources*, vol. 110, no. 2, pp. 321–329, 2002.
- [18] H. Fang, Y. Wang, and J. Chen, "Health-aware and user-involved battery charging management for electric vehicles: Linear quadratic strategies," *IEEE Transactions on Control Systems Technology*, vol. 25, no. 3, pp. 911–923, 2017.
- [19] H. Fang, C. Depcik, and V. Lvovich, "Optimal pulse-modulated lithium-ion battery charging: Algorithms and simulation," *Journal of Energy Storage*, vol. 15, pp. 359–367, 2018.
- [20] M. Sitterly, L. Y. Wang, G. G. Yin, and C. Wang, "Enhanced identification of battery models for real-time battery management," *IEEE Transactions on Sustainable Energy*, vol. 2, no. 3, pp. 300–308, 2011.
- [21] J. F. Van Doren, S. G. Douma, P. M. Van den Hof, J. D. Jansen, and O. H. Bosgra, "Identifiability: from qualitative analysis to model structure approximation," *Proceedings of the 15th IFAC Symposium on System Identification*, vol. 42, no. 10, pp. 664–669, 2009.
- [22] H. Fang, Y. Wang, Z. Sahinoglu, T. Wada, and S. Hara, "State of charge estimation for lithium-ion batteries: An adaptive approach," *Control Engineering Practice*, vol. 25, pp. 45–54, 2014.
- [23] N. Tian, Y. Wang, J. Chen, and H. Fang, "On parameter identification of an equivalent circuit model for lithium-ion batteries," in *IEEE Conference on Control Technology and Applications (CCTA)*, 2017, pp. 187–192.
- [24] "The EPA Urban Dynamometer Driving Schedule (UDDS) [Online]," Available: <https://www.epa.gov/sites/production/files/2015-10/uddscol.txt>.